2026 IEEE International Conference on Robotics and Automation (ICRA 2026)
June 1-5, 2026. Vienna, Austria

A Modular, Wireless and Wearable Biosignal Acquisition Platform

Antonios Doukakis[1], Aikaterini Smyrli[2], Makis Livadas[3], Henrique De Melo Ribeiro[3], Shadiya Alingal Meethal[4], Mohamad Reza Shahabian Alashti[4], Gabriella Lakatos[4], Patrick Holthaus[4] and Farshid Amirabdollahian[4]

***Abstract*— We present a modular, wireless biosignal acquisition platform designed to enable scalable electromyography (EMG) and inertial measurement unit (IMU) sensing for wearable robotics applications. The system supports up to 64 EMG channels and integrates a 9-axis IMU, leveraging a distributed Leader-Follower board architecture. In this work, we demonstrate synchronised acquisition of 32 EMG channels together with IMU motion data in a fully wireless setup. The embedded firmware ensures low-latency, high-fidelity streaming at 1.4 kHz over a 2.4-GHz industrial, scientific and medical (ISM) band link. Benchmarking shows that the platform maintains uniformly strong performance across noise, power, footprint, bandwidth, and scalability, in contrast to existing designs that optimize only a single metric. Experimental demonstrations confirm reliable acquisition of high-density EMG and IMU signals across functional activities, highlighting the device's robustness and wearability. The proposed system provides a compact and flexible solution for intent-aware wearable technologies, with applications in assistive exosuits, rehabilitation, and human–robot interaction.**

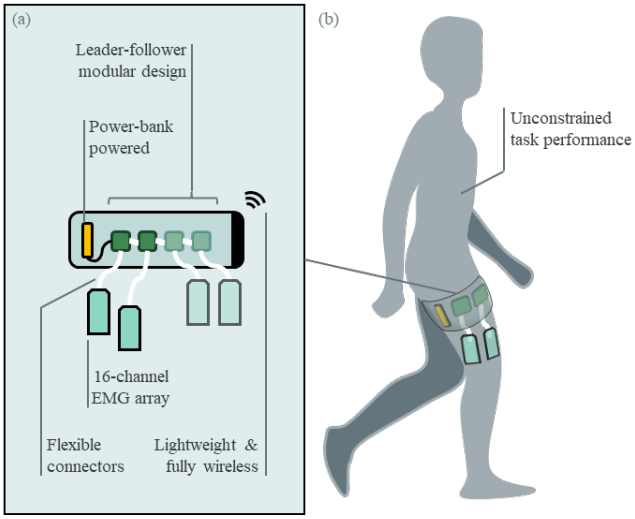

Fig. 1. System overview and wearable deployment.

I. Introduction

Wearable assistive robotics has gained substantial interest due to its potential to enhance mobility, rehabilitation outcomes, and overall quality of life for individuals facing motion impairments. The effective deployment of wearable robotic solutions, such as in exoskeletons and soft exosuits, critically depends on accurate, real-time detection of motion kinetics and user intent. Among various biosignals used for motion recognition, surface electromyography (EMG) and inertial measurement unit (IMU) data have emerged as reliable sources due to their sensitivity to muscle activation and kinematic states, respectively.

A limitation of traditional EMG sensors is their dependence on electrode placement [1]. The use of High-Density surface EMG (HD-EMG) arrays provides a solution to this problem, allowing the detection of not only the temporal but also of the spatial distribution of muscle activity [2], that can be used to decode motor unit firing events [3] and thus help in the accurate estimation of muscle forces and intended motion [4].

Traditional medical-grade systems are usually tethered and offer excellent signal quality and channel counts (as high as 128 channels in the Refa and SAGA platforms). However, they remain bulky, power-demanding, and are constrained by wired leads, limiting user mobility and introducing motion artifacts from cable sway [5]. On the other hand, a variety of commercial and research-grade wearable EMG and HD-EMG systems have emerged to deliver high-fidelity biosignal acquisition outside the lab [6]–[17].

EMG sensing is inherently susceptible to noise due to the low power of the measured bio-potential. Increased noise levels may originate from muscle crosstalk, high impedance in the skin-electrode interface, artifacts due to cable sway, and even interference from ambient electro-magnetic fields [5], [18], [19]. Low-channel-count wearable myosensing modules (up to 8 channels) have achieved sub-μV noise floors with low power budgets, enabling small form factors, but their limited spatial resolution constrains the decoding of complex, multi-muscle patterns [8]. High-density research amplifiers (up to 128 channels) now demonstrate the feasibility of small, stacked modules with per-module noise less than 0.4 μV_{RMS} and real-time wireless streaming, though they typically occupy tens of square centimeters (2.5 cm^2/channel) and require considerable power ($\approx$ 57.8 mW/channel) [10]. Even though portable, these devices are power-demanding and lack dynamic transparency due to their weight and form factor. A fully wearable wireless solution has been presented in [20], reporting a 0.3 cm^2/channel footprint and a power consumption of 18.8 mW/channel, however, the signal noise is measured at 1.8 μV_{RMS}. Similarly [9] reports a footprint of 0.4 cm^2/channel with a significant power reduction at 1.8 mW/channel, at the cost of a further noise increase at

*Corresponding author.
[1]A.D. and A.S. are with Tech Hive Labs and with the National Technical University of Athens, Greece.
[2]A.S. is also with the Athena RC Robotics Institute, Greece.
[3]M.L. and H.R. are with the Brunel Innovation Centre (BIC), UK
[4]S.A.M., M.S.A., G.L., P.H. and F.A. are with the University of Hertfordshire, UK

2.4 μV_{RMS}. It is evident that existing platforms trade off signal quality, channel count, battery life, and wearability differently. This highlights the need for a truly wearable HD-EMG system that combines low noise, real-time multi-muscle data streaming, reduced don-and-doff complexity, and extremely low cost.

To address these needs, this paper presents a novel modular wireless biosignal acquisition platform built upon a distributed Leader–Follower multi-board architecture, enabling scalable high-density EMG acquisition with synchronized IMU integration. The system supports wireless communication and real-time multimodal data streaming within a compact wearable form factor. The design specifically accommodates modular scalability, supporting a variable number of EMG channels that can be tailored to individual application requirements. Additionally, our platform supports both bipolar EMG and HD-EMG acquisition, providing flexibility to address the trade-off between performance and usability in EMG system design [2].

To validate the effectiveness and practical utility of the proposed architecture, synchronised HD-EMG and IMU acquisition is demonstrated using a 32-channel configuration in fully wireless operation. These results highlight the feasibility of scalable multimodal biosignal streaming in a wearable setup and establish the platform as an enabling foundation for future intent-aware wearable robotic pipelines.

The remainder of this paper is structured as follows: Section II details the system architecture, while Section III analyzes the board design. Section IV presents the board performance, including benchmarking and synchronised HD-EMG and IMU demonstrations across representative daily-life activities. Section V discusses the results, and Section VI concludes the paper.

II. System Architecture Overview

The proposed platform is a modular, body-worn system for high-density EMG and IMU acquisition (Fig. 1). Its small form factor, comfortable placement, and low power draw make it well-suited to wearable applications.

The system consists of one Leader board and up to three Follower boards. Each board integrates a 16-channel EMG analog front end (AFE) and an STM32WB55 low-power dual-core microcontroller (MCU) with an integrated 2.4-GHz radio for wireless communication. Motion sensing is provided on the Leader via an integrated 9-axis IMU.

By interconnecting boards in a Leader–Follower configuration (Fig. 2), the architecture scales from 16 to 64 EMG channels. Flexible ribbon connectors allow the boards to be distributed across the body to accommodate contours and reduce wiring complexity. The Leader simultaneously acquires its own 16 EMG channels and IMU data while aggregating EMG streams from attached Followers.

Two acquisition modes are supported. In the wireless mode (blue in Fig.2, used in this work), the Leader collects data from Followers over high-speed SPI and forwards the aggregated stream in real time to a USB dongle via a custom low-latency wireless link. In the wired mode (red in Fig.2), a USB hub integrated on the Leader enables parallel data acquisition for applications that demand higher throughput. This dual-mode, modular architecture provides synchronised multi-channel recording while preserving mobility and comfort in wearable scenarios.

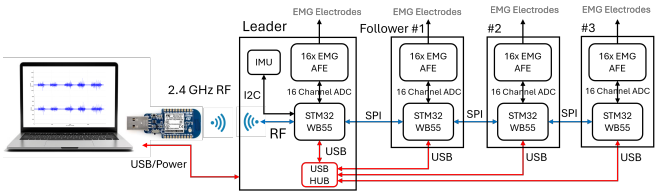

Fig. 2. System Architecture. The system integrates two distinct communication protocols for wireless (blue) and wired (red) inter-board communication.

III. Board Design

The modular system is designed to accommodate the AFE for EMG acquisition across multiple boards, while only the Leader board hosts the hardware necessary for motion sensing and supporting functionalities (IMU, inter-board and external communication, etc.) in a minimal spatial configuration. The board design is discussed in this section.

A. Analog Front End (AFE)

The AFE of the proposed system, shown in Fig. 3, employs a low cost, low power and low-noise instrumentation amplifier (INA317) with a gain of 23 V/V (set by its R_g resistor), a common-mode rejection ratio (CMRR) $>$ 110 dB for mains interference suppression, and an input impedance exceeding 100 GΩ $\|$ 3 pF to avoid electrode loading. A passive RC AC-coupling network at the INA317 inputs removes electrode DC offsets, while precision component selection ensures input symmetry and minimizes CMRR degradation.

The INA317 operates from a 3.3 V supply with its reference (REF) pin biased at half the rail, thereby offsetting the amplified EMG signal. The final stage, designed for anti-aliasing, is a second-order Sallen-Key low-pass filter with a gain of 22 V/V (set by $1 + R_5/R_6$ at higher frequencies) and a simulated cutoff frequency of 286 Hz. The inclusion of capacitor C_5 in the feedback path enforces unity gain at low frequencies, preventing further amplification of the EMG signal's DC offset.A similar approach has been described in detail in [21]. In combination with the input AC-coupling stage, C_5 forms a second-order high-pass filter with

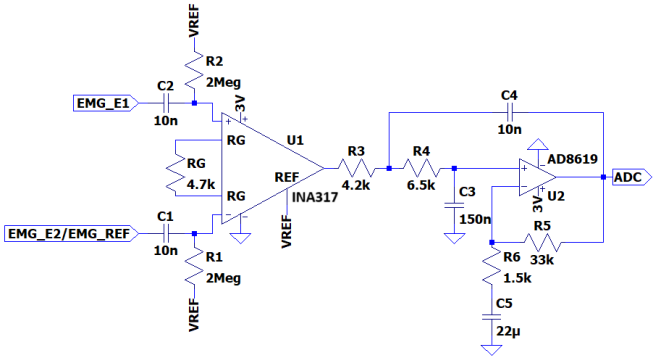

Fig. 3. EMG signal acquisition analog front-end unit. Each board hosts 16 instances of the EMG AFE unit.

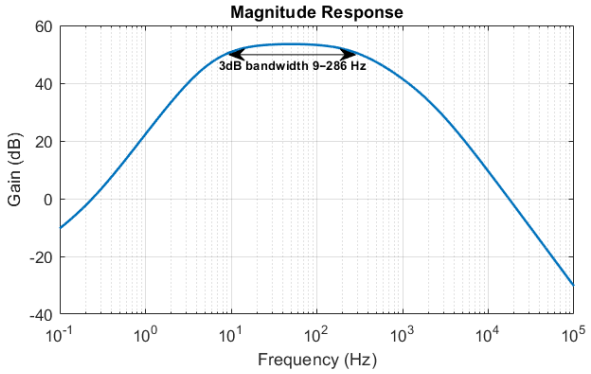

Fig. 4. Magnitude response of the EMG AFE.

a simulated cutoff frequency of 9 Hz. The overall magnitude response of the AFE is shown in Fig. 4, indicating a $-3\,\mathrm{dB}$ bandwidth of 9–286 Hz.

B. Supporting Hardware

The Leader and Follower boards are illustrated in Figs. 5 and 6. Each board features a compact footprint of 45.5 mm $\times$ 48 mm, making the design well suited for unobtrusive wearable integration. The boards share a common architectural basis: both are built around an STM32WB55 MCU, and each includes a USB-C port primarily for programming and firmware debugging. For electrode interfacing, every board provides two EMG ribbon terminals (one per side), yielding 16 EMG electrode terminals per board. Accordingly, each board incorporates 16 EMG AFE units (as described previously) for signal pre-processing.

To enable full operation regardless of the number of Followers attached, the Leader implements select additions: it carries one inter-board ribbon connector to interface with any connected Followers and retains auxiliary sensing components omitted on Followers: namely, the 9-axis IMU, the USB hub controller IC, and the PCB antenna. By contrast, each Follower exposes two inter-board communication ribbon terminals to support a modular, expandable daisy-chain configuration, while omitting the IMU, USB hub controller IC, and PCB antenna present on the Leader.

The Leader's 9-axis IMU is the BNO086 system-in-package (SiP), which integrates a 3-axis accelerometer, gyroscope, and magnetometer, plus an embedded microcontroller running sensor-fusion firmware. It provides multiple orientation outputs; in the typical configuration, accelerometer, gyroscope, and magnetometer data are fused to produce an absolute rotation vector referenced to magnetic north and gravity, reported in quaternion format. The device interfaces with the Leader's STM32WB55 MCU over I^2C and supports rotation-vector update rates up to 400 Hz.

The Leader integrates a Microchip USB2514B USB interface IC, a hub controller which is fully compliant with the USB 2.0 specification and supports Full-Speed operation. This selection provides four downstream ports: one port is permanently assigned to the Leader board, while the remaining three are reserved for any Follower boards.

The PCB antenna is implemented as a meandered inverted-F antenna (MIFA), selected for its compact size, low cost,

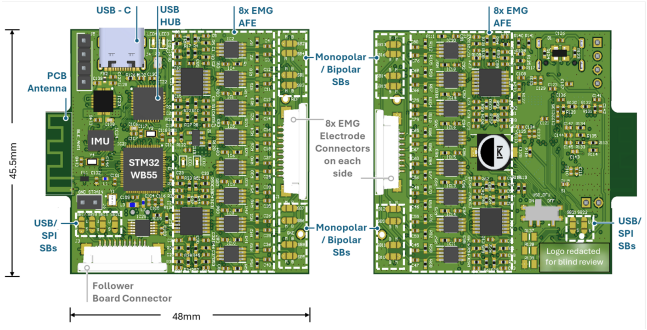

Fig. 5. Leader Board: top view (left) and bottom view (right).

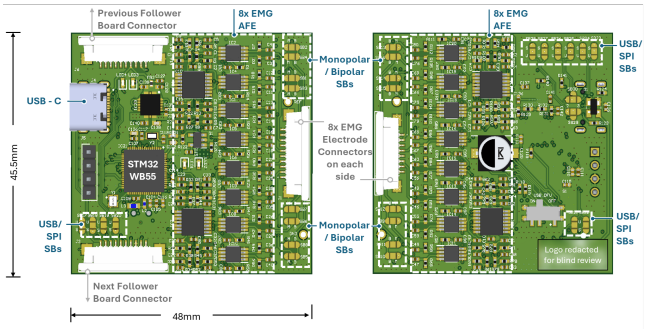

Fig. 6. Follower Board: top view (left) and bottom view (right).

and effective performance in the 2.4 GHz ISM band. Since a relatively long communication range is not a requirement for this application, the MIFA provides an ideal solution for wearable devices where small form factor and integration simplicity are prioritized. Careful impedance matching to 50 Ω was performed during PCB design to ensure proper antenna performance.

C. Conformable, Modular and Customizable Design

Accommodating diverse body contours requires a comfortable hardware design. The platform's modular, compact form factor minimizes on-site volume and permits distributing device bulk across non-deformable body segments. Flexible ribbon cables provide inter-board links and connect the EMG electrodes, avoiding stiff connections that could impede user mobility.

The boards support monopolar and bipolar acquisition via solder-bridge (SB) selection logic (Figs. 5 and 6). In monopolar mode, each AFE uses one active electrode referenced to a common REF shared across all channels. In bipolar mode, the AFE connects to a pair of active electrodes, directly measuring their potential difference. Overall, the system can interrogate up to 64 monopolar channels or 32 bipolar channels, depending on the use case.

Per-use-case customization is further enabled at the serial bus interface. Followers communicate with the Leader either over SPI, with data routed to the Leader's SoC for wireless transmission, or over USB, where Followers connect in parallel through the Leader-integrated USB hub. The mode is selected via SPI/USB SBs (Figs. 5 and 6). In wired operation, the integrated hub uses the Leader's USB-C port to establish the connection to the PC.

D. Embedded Firmware

Distributed firmware executes on the Leader and Follower boards: each node performs local ADC and sample timing, while the Leader orchestrates inter-board data collection, aggregation, and wireless transmission. This architecture ensures synchronised EMG sampling across boards and natively accommodates auxiliary sensing modalities.

Each node executes ADC conversions and reads the most recent sample at a fixed service cadence. Follower boards forward samples to the Leader over 16 MHz SPI. Although the STM32WB55 integrates a 12-bit ADC, in this design we exploit its hardware oversampling feature, which yields an effective resolution of 16 bits. Compared to implementations that rely on native 16-bit ADCs [9], [20], this approach improves noise performance and quantization fidelity.

The Leader polls Followers sequentially, aggregates EMG samples, encapsulates them, and transmits packets over a low-latency wireless link. This link is implemented directly on the 2 Mbps Bluetooth Low Energy (BLE) physical layer using STMicroelectronics' dedicated API, enabling fine-grained control of timing and packetization. Our implementation adopts a custom protocol rather than standard BLE profiles to reduce overhead and latency. A similar wireless architecture was reported in [9]; however, that system employed an external RF transceiver, whereas here the STM32WB55's integrated radio co-processor handles wireless communication.

The Leader also acquires orientation from the onboard IMU via the I^2C interface and integrates it into the transmitted dataset, unifying electrophysiological and motion information in a single stream. Ultimately, throughput on the wireless link bounds streaming performance, limiting the sampling rate to an inter-sample interval of 0.7 ms ($\approx$1.43 kHz) for the given payload. For more demanding applications, the wired configuration via the Leader's integrated USB hub permits higher sampling rates; in our setup, we achieved $\geq$ 4kHz over USB.

IV. Board Performance

To showcase the platform under its intended use, we adopt the wireless monopolar configuration with one Leader and one Follower, yielding 32-channel HD-EMG with synchronized IMU. We then evaluate board-level performance by quantifying input-referred noise (IRN), benchmarking key metrics against representative systems, and demonstrating practical applicability through daily-life activity recordings.

A. Noise Performance Evaluation

We first establish the proposed AFE's baseline fidelity by quantifying its IRN. Since EMG amplitudes are inherently low, the IRN of the AFE is a critical benchmark, as it affects the smallest detectable muscle activations and ultimately constrains signal fidelity.

The IRN of the proposed AFE was measured by shorting the INA317's active and reference inputs to system ground and recording the ADC output at 2 kHz for 10 s over the wired USB interface, following the procedure described

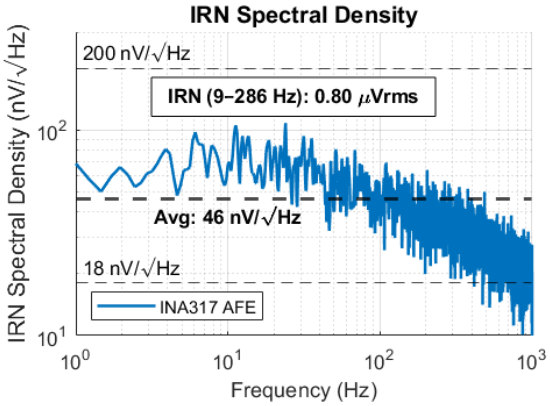

Fig. 7. AFE Noise Performance, IRN Spectral Density.

in [10]. In the same study, the commercial Quattrocento system (OT Bioelettronica) exhibited a noise density of approximately 200 nV/$\sqrt{\text{Hz}}$, while the study's custom amplifier achieved 18 nV/$\sqrt{\text{Hz}}$. Our system achieves a similarly favorable noise performance at an average of 48 nV/$\sqrt{\text{Hz}}$, as depicted in Fig. 7, which illustrates its placement relative to these systems. The root mean square (RMS) value of the IRN calculated by:

$$\text{IRN}_{\text{RMS}}\,[\text{V}] = \sqrt{\int_{f_1}^{f_2} \left(\text{IRN}(f)\right)^2 \, df} \qquad (1)$$

evaluates at $\text{IRN}_{\text{RMS}} = 0.8\mu V_{\text{RMS}}$ for our study, while reported values in relevant literature are given in Table I.

B. Performance Benchmarking

A comparison of the proposed system's performance with other EMG acquisition platforms is summarized in Table I. Existing designs tend to optimize one attribute while exhibiting extremes in others: for example, MyoLink [10] attains an exceptionally low noise floor ($<$ 0.4 μV_{RMS}) but at the cost of high power (57.8 mW/channel) and large area (2.5 cm^2/channel); Cerone et al. [20] achieve very compact hardware (0.3 cm^2/channel) with increased power (18.8 mW/channel) and reduced noise performance (1.8 μV_{RMS}); Tam et al. [9] minimize power (1.8 mW/channel) and size (0.4 cm^2/channel), but compromise noise performance (2.4 μV_{RMS}) and have a lower sampling rate (1 kHz).

In contrast, our platform avoids isolated optima: across the performance metrics considered - sampling frequency (1.4 kHz wireless; higher in wired mode), effective resolution (16-bit via oversampling), IRN (0.8 μVRMS),

TABLE I: Benchmarking comparison with related works.

Parameter	Units	This work**	[10]	[20]	[9]
Maximum Bandwidth	[Hz]	9–286	23-0.26xFS*	10-500	20-500
Resolution	[bits]	16	24	16	16
Dynamic Range	[mVpp]	3.3	42	10	10
Sampling Frequency	[kHz]	1.4	1-8	2	1
DC Offset Tolerance	[mV]	AC-Coupled	600	-	-
RMS IRN	[μV]	0.8	$<$0.4	1.8	2.4
Unipolar Channels	[-]	16-64	32-128	32	32
Bipolar Channels	[-]	32	-	-	-
CMRR @ 50 Hz	[dB]	110	$>$110	82	82
Input Resistance	[GΩ]	$>$100	$>$100	1.3	1.3
Area per Channel	[cm^2]	1.37	2.5	0.3	0.4
Wireless Protocol	[-]	Radio	Wired	WiFi	Radio
Power per Channel	[mW]	6.125	57.8	18.8	1.8

*FS = Sampling Frequency, **Refers to the wireless unipolar configuration

CMRR (110 dB), input resistance ($>$ 100 GΩ), power (6.1 mW/channel), and area (1.37 cm^2/channel) - we maintain uniformly strong performance without any outlier weaknesses. The slightly narrower bandwidth (9–286 Hz) is not limiting, as most EMG energy lies below 250 Hz [22], and it further helps suppress aliasing at a 1.4 kHz sampling rate. This balanced profile, together with modular support for 64-channel monopolar or 32-channel bipolar acquisition, IMU sensing, and wired/wireless operation, translates into a practically effective, truly wearable HD-EMG platform rather than a device tuned to a single headline metric.

C. Representative activity segments

To validate the signal quality of our custom acquisition board, we recorded high-density EMG (HD-EMG) and synchronised IMU data during eight daily-life activities: *Sitting*, *Standing*, *Walking*, *Sitting Down*, *Standing Up*, *Turn*, *Stairs Up*, and *Stairs Down*. Activity onset/offset times were annotated in the experiment log and used to extract fixed-length windows (2–4 s per task).

a) HD-EMG.: Fig. 8 shows the HD-EMG signals recorded from a 32-channel electrode array placed over the right *vastus lateralis* and *rectus femoris*. To improve visibility, each channel was demeaned, lightly smoothed with a causal moving average ($W_{\mathrm{EMG}} \approx 20\,\mathrm{ms}$), and amplitudes were magnified ($\times 3$) relative to their local baseline. All 32 channels are overlaid in each subplot, revealing activity-specific bursts and recruitment patterns. Importantly, *Sitting* and *Sitting Down*, and *Standing* and *Standing up* are captured as distinct tasks, showing different temporal dynamics despite similar muscle groups.

b) IMU orientation.: Fig. 9 presents the corresponding IMU orientation, computed from the unit quaternions provided by the on-board BNO086 sensor. Quaternions $q = (q_0, q_1, q_2, q_3)$ were converted to Euler angles (ϕ, θ, ψ) in the 'xyz' sequence (roll, pitch, yaw), expressed in degrees. A short moving average ($W_{\mathrm{IMU}} \approx 100\,\mathrm{ms}$) was applied for clarity. The orientation traces align with the EMG bursts, confirming synchronization between modalities and highlighting task-dependent kinematic changes (e.g., clear pitch variations during stair ascent/descent).

c) Results narrative.: Looking at *Sitting*, the HD-EMG exhibits uniformly low amplitude and minimal fluctuations across all 32 channels, consistent with low quadriceps recruitment. The IMU angles are stable (yaw $\sim$50°, roll $\sim$–5°, pitch $\sim$18°), indicating a quasi-static seated posture. Moving to *Standing*, EMG amplitude increases with clearer tonic activity across channels, and the IMU orientation shifts substantially (yaw $\sim$–120°, roll $\sim$120°, pitch $\sim$–35°), reflecting the change from seated to upright alignment. During *Walking*, EMG amplitudes remain comparable to Standing but show stronger temporal modulation with alternating bursts characteristic of cyclical right-leg activation (electrodes placed over the right quadriceps). The IMU roll/pitch traces oscillate periodically in step with the gait cycle, while the mean orientation envelope remains close to Standing.

Transitions, *Sitting Down* and *Standing Up*, display short, high-contrast EMG bursts aligned with discrete angular transitions in the IMU, consistent with eccentric and concentric quadriceps activation, respectively. *Turn* produces moderate EMG bursts with a characteristic yaw deviation, while *Stairs Up* and *Stairs Down* show higher and more prolonged EMG bursts across channels (greater load demand) accompanied by pronounced pitch excursions that differentiate ascent from descent. Overall, the synchronised changes across EMG and IMU confirm correct acquisition and timing, and they reveal task-dependent neuromuscular and kinematic signatures useful for downstream intent detection.

V. Discussion

The proposed acquisition platform demonstrates that portable and power-efficient biosignal sensing can be achieved without compromising signal fidelity or wearability.

A key strength of the system lies in its modularity: Leader and Follower boards can be distributed across different body regions and channel count can be scaled to meet application-specific requirements, while preserving a plug-and-play setup with minimal don/doff complexity. Flexible ribbon interconnects allow the system to conform to diverse body contours, facilitating electrode placement across multiple muscle groups. This flexibility is particularly relevant for wearable robotics, where different control pipelines may require sparse or dense sensing depending on the task.

The platform was evaluated through benchmarking experiments and comparisons with the state-of-the-art. The combination of low input-referred noise, high input resistance, and strong CMRR ensures that subtle EMG activity remains detectable even in real-life conditions, while the unified wireless link eliminates motion artifacts associated with cable sway. Compared to prior work in the literature, our design balances input fidelity, power consumption, scalability and wearability, avoiding the extreme trade-offs observed in other systems. This balanced profile makes it particularly well-suited for wearable robotics, where reliability, comfort, and energy efficiency must coexist.

The analog bandwidth of 9-286 Hz covers the dominant EMG spectral content used in intent detection and most myographic analyses [23]. This choice ensures efficient use of resources without loss of relevant physiological information. Importantly, the bandwidth is not fixed: it can be readily adjusted through component tuning when applications require different passbands.

While these hardware-level results provide strong evidence of signal fidelity, their impact is most clearly demonstrated in synchronized EMG-IMU recordings of daily life activities.

Specifically, the experimental demonstrations highlight that the proposed system reliably captures both high-density EMG activity and concurrent IMU orientation signals across a range of functional tasks. In the HD-EMG recordings (Fig. 8), distinct bursts corresponding to muscle activation patterns can be clearly identified for dynamic activities such as walking, stair ascent/descent, and sit-to-stand transitions. The

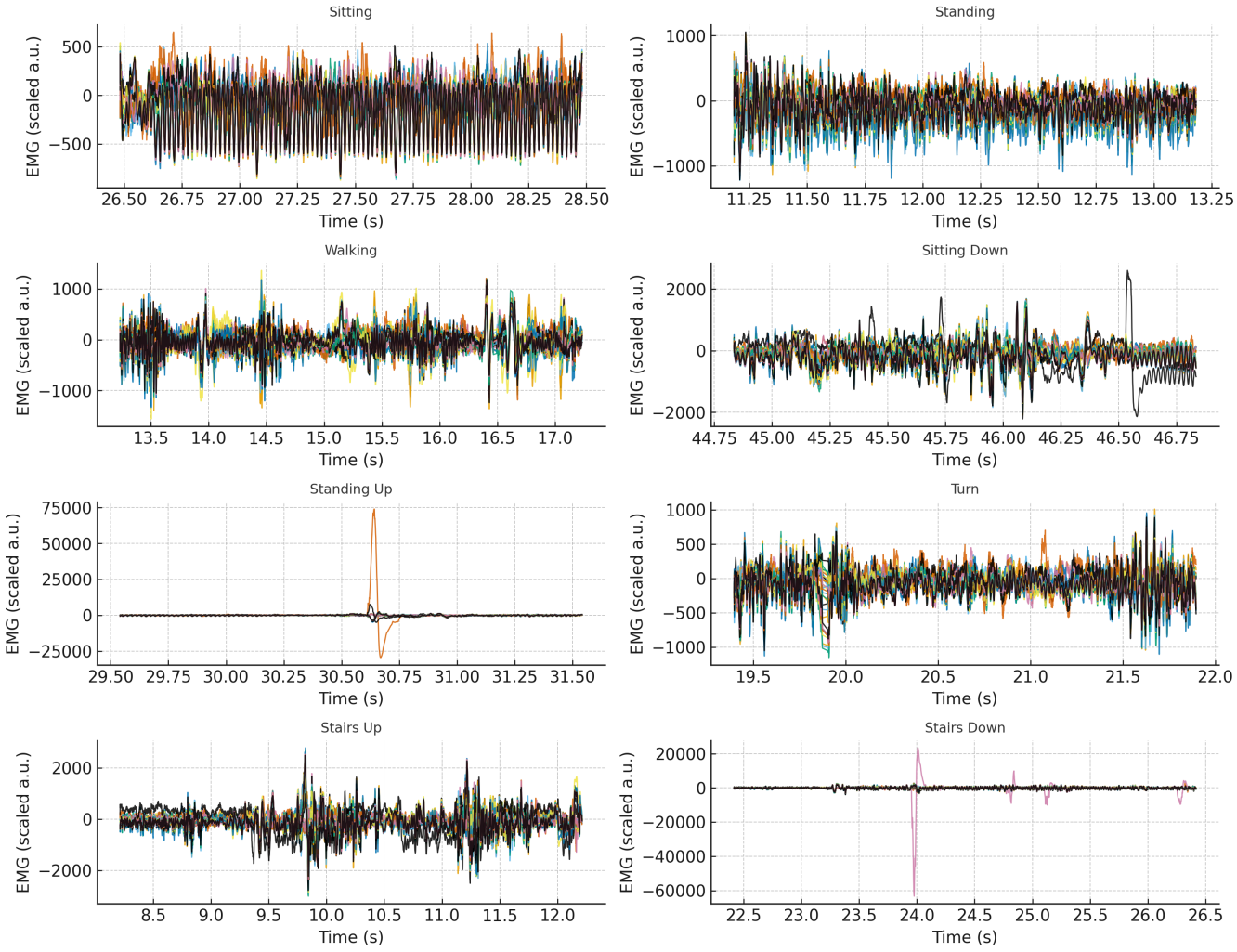

Fig. 8. HD-EMG across 32 channels (overlaid, smoothed $\sim$20 ms, $\times$3 magnification) during eight representative activities.

synchronised IMU traces (Fig. 9) confirm consistent kinematic alignment, showing smooth pitch and roll variations during gait cycles and sharp transitions during turning and sit-stand motions. Importantly, the acquisition board supports both bipolar and high-density EMG configurations, providing flexibility for diverse experimental and clinical applications. It is worth noting that the apparent discontinuities in the IMU orientation traces around $\pm 180^{\circ}$ result from the wraparound property of Euler angle representations rather than sensor artifacts. Continuous quaternion streams provided by the BNO086 or unwrapped Euler trajectories can be used in downstream processing to avoid these jumps when smooth orientation trajectories are required.

These results underline the system's ability to capture multimodal biosignals without the motion artifacts typically associated with tethered setups. The clean onset/offset structure of the EMG bursts during performed activities demonstrates both the low noise floor and the benefit of the chosen 9-286 Hz bandwidth, which preserves physiologically relevant spectral content while filtering low-frequency drift. The coherence between EMG and IMU data further illustrates the platform's suitability for intent-aware pipelines, where electrophysiological and kinematic cues need to be jointly processed in real time.

This work established a strong baseline in controlled, single-user daily-life activities trials using a 32-channel configuration of the modular system. Future work will extend validation to multi-user cohorts and curate rigorously annotated, fully untethered 64 channel EMG and synchronised IMU datasets from out-of-laboratory activities, toward fully autonomous, closed-loop operation with real-time intent classification.

VI. Conclusion

In this work, we introduced a modular, wireless biosignal acquisition platform that combines scalable EMG sensing with integrated IMU sampling in a compact, wearable form factor. By prioritizing modularity, scalability, and usability, this work establishes a practical foundation for next-generation wearable biosignal interfaces.

The platform achieves low noise, a small footprint, high CMRR, low per-channel power consumption, and overall a balanced, strong performance profile across evaluation

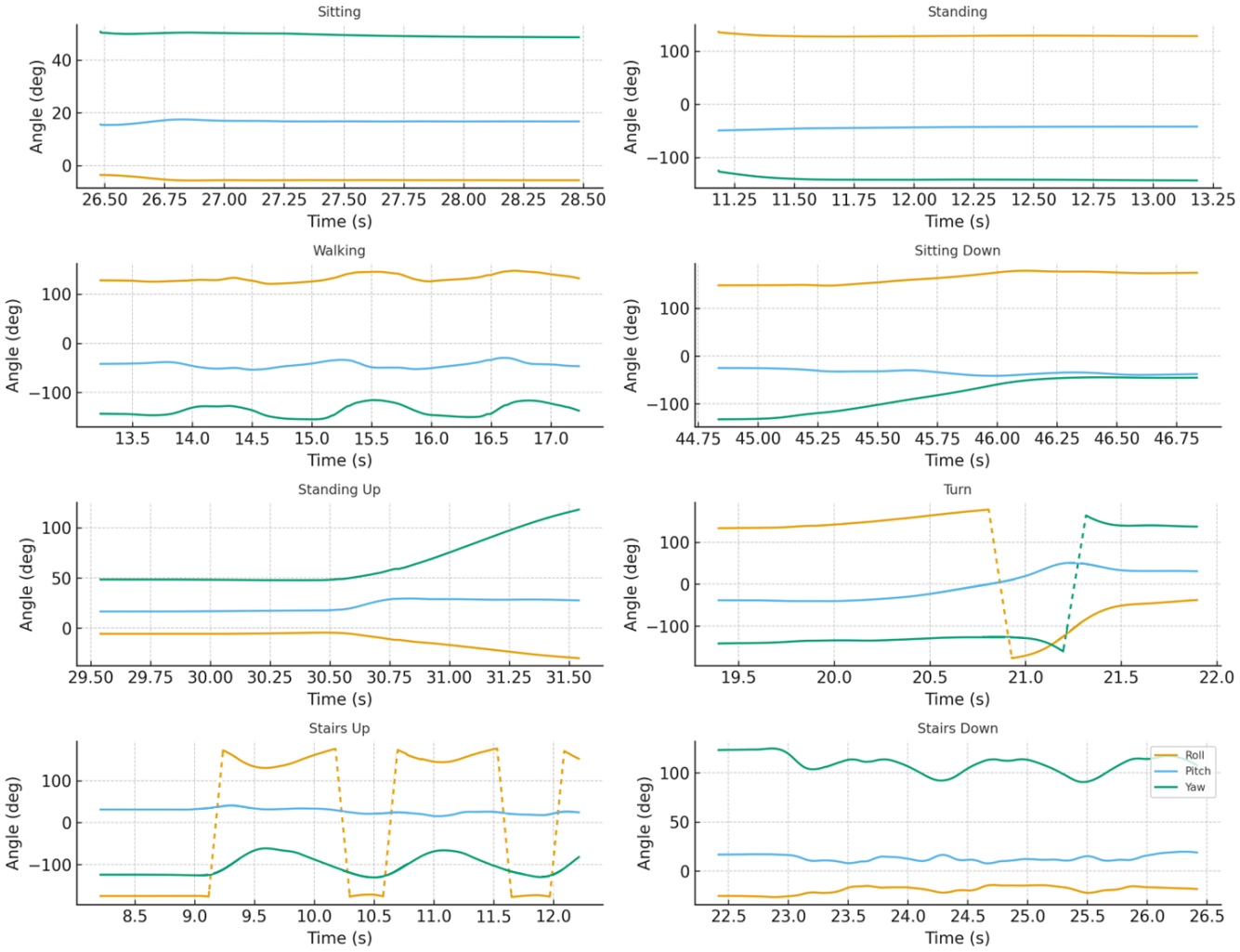

Fig. 9. IMU orientation (Euler angles roll/pitch/yaw, smoothed ∼100 ms) during the same activities and time windows as Fig. 8. Dashed lines indicate data discontinuities due to ±180° angle wrapping.

metrics, while supporting up to 64 EMG channels in a Leader-Follower configuration. Demonstrations of biosignal acquisition during representative daily-life activities validate the system's robustness and highlight its suitability for wearable applications where unobstructed mobility is essential.

Beyond benchmarking, the platform lays the groundwork for intent-aware control pipelines by delivering high-quality multimodal data in real time. The unified wireless streaming of EMG and IMU data enables robust intent-aware pipelines that benefit from the joint exploitation of electrophysiological and kinematic signals. Future work will extend evaluation to multi-user studies, and target real-time intent detection based on the promising initial results.

ACKNOWLEDGMENT

This work was supported by the European Union's Horizon Europe programme through the SWAG Project under Grant 101120408 and by Horizon Europe UK Research and Innovation (UKRI) under the UK government's Horizon Europe funding guarantees 10079504 and 10087684.

REFERENCES

[1] L. Mesin, R. Merletti, and A. Rainoldi, "Surface EMG: The issue of electrode location," *Journal of Electromyography and Kinesiology*, vol. 19, no. 5, pp. 719–726, 2009, ISSN: 1050-6411. DOI: 10.1016/j.jelekin.2008.07.006.

[2] T. Sugiarto, C.-L. Hsu, C.-T. Sun, W.-C. Hsu, S.-H. Ye, and K.-T. Lu, "Surface EMG vs. high-density EMG: Tradeoff between performance and usability for head orientation prediction in vr application," *IEEE Access*, vol. 9, pp. 45 418–45 427, 2021. DOI: 10.1109/ACCESS.2021.3067030.

[3] A. Gogeascoechea, M. I. Mohamed Refai, U. S. Yavuz, and M. Sartori, "Towards real-time decoding of motor unit firing events and resulting muscle activation during human locomotion and high-force contractions," in *2024 10th IEEE RAS/EMBS International Conference for Biomedical Robotics and Biomechatronics (BioRob)*, 2024, pp. 1434–1439. DOI: 10.1109/BioRob60516.2024.10719929.

[4] D. Farina, F. Negro, S. Muceli, and R. M. Enoka, "Principles of motor unit physiology evolve with advances in technology," *Physiology (Bethesda)*, vol. 31, no. 2, pp. 83–94, Mar. 2016. DOI: 10.1152/physiol.00040.2015.

[5] E.-R. Symeonidou, A. D. Nordin, W. D. Hairston, and D. P. Ferris, "Effects of cable sway, electrode surface area, and electrode mass on electroencephalography signal quality during motion," *Sensors*, vol. 18, no. 4, p. 1073, Apr. 2018. DOI: 10.3390/s18041073.

[6] R. F. Yazicioglu, P. Merken, R. Puers, and C. Van Hoof, "A 60 μw 60 nv/$\sqrt{}$hz readout front-end for portable biopotential acquisition systems," *IEEE Journal of Solid-State Circuits*, vol. 42, no. 5, pp. 1100–1110, 2007. DOI: 10.1109/JSSC.2007.894804.

[7] U. Barone and R. Merletti, "Design of a portable, intrinsically safe multichannel acquisition system for high-resolution, real-time processing hd-sEMG," *IEEE Transactions on Biomedical Engineering*, vol. 60, no. 8, pp. 2242–2252, 2013. DOI: 10.1109/TBME.2013.2252346.

[8] K. Petkos, S. Koutsoftidis, T. Guiho, and et al., "A high-performance 8 nv/$\sqrt{\text{Hz}}$ 8-channel wearable and wireless system for real-time monitoring of bioelectrical signals," *Journal of NeuroEngineering and Rehabilitation*, vol. 16, p. 156, 2019. DOI: 10.1186/s12984-019-0629-2.

[9] S. Tam, G. Bilodeau, J. Brown, G. Gagnon-Turcotte, A. Campeau-Lecours, and B. Gosselin, "A wearable wireless armband sensor for high-density surface electromyography recording," in *2019 41st Annual International Conference of the IEEE Engineering in Medicine and Biology Society (EMBC)*, 2019, pp. 6040–6044. DOI: 10.1109/EMBC.2019.8857750.

[10] S. Koutsoftidis, D. Y. Barsakcioglu, K. Petkos, D. Farina, and E. M. Drakakis, "Myolink: A 128-channel, 18 nV/$\sqrt{\text{Hz}}$, embedded recording system, optimized for high-density surface electromyogram acquisition," *IEEE Transactions on Biomedical Engineering*, vol. 69, no. 11, pp. 3389–3396, 2022. DOI: 10.1109/TBME.2022.3170025.

[11] K. Ann Ng, L. Zhang, H. Wu, T. Tang, and J. Yoo, "A single-stage, capacitively-coupled instrumentation amplifier with complementary transimpedance boosting," *IEEE Transactions on Circuits and Systems I: Regular Papers*, vol. 71, no. 7, pp. 2989–3001, 2024. DOI: 10.1109/TCSI.2024.3391169.

[12] M. Ergeneci, K. Gokcesu, E. Ertan, and P. Kosmas, "An embedded, eight channel, noise canceling, wireless, wearable sEMG data acquisition system with adaptive muscle contraction detection," *IEEE Transactions on Biomedical Circuits and Systems*, vol. 12, no. 1, pp. 68–79, 2018. DOI: 10.1109/TBCAS.2017.2757400.

[13] G. L. Cerone and M. Gazzoni, "A wireless, minaturized multi-channel sEMG acquisition system for use in dynamic tasks," in *2017 IEEE Biomedical Circuits and Systems Conference (BioCAS 2017) - Proceedings*, Turin, Italy: IEEE, 2017, pp. 1–4. DOI: 10.1109/BIOCAS.2017.8325129.

[14] Y.-H. Yang, S.-J. Ruan, P.-C. Chen, Y.-H. Liu, and Y.-H. Hsueh, "A low-cost wireless multichannel surface EMG acquisition system," *IEEE Consumer Electronics Magazine*, vol. 9, no. 5, pp. 14–19, 2020. DOI: 10.1109/MCE.2020.2986792.

[15] J. Fu, J. Chen, Y. Shi, and Y. Li, "Design of a low-cost wireless surface EMG acquisition system," in *2013 6th International IEEE/EMBS Conference on Neural Engineering (NER)*, 2013, pp. 699–702. DOI: 10.1109/NER.2013.6696030.

[16] G. Biagetti, P. Crippa, L. Falaschetti, S. Orcioni, and C. Turchetti, "A portable wireless semg and inertial acquisition system for human activity monitoring," in *Bioinformatics and Biomedical Engineering*, Cham: Springer International Publishing, 2017, pp. 608–620. DOI: 10.1007/978-3-319-56154-7_54.

[17] D. Brunelli, E. Farella, D. Giovanelli, B. Milosevic, and I. Minakov, "Design considerations for wireless acquisition of multichannel sEMG signals in prosthetic hand control," *IEEE Sensors Journal*, vol. 16, no. 23, pp. 8338–8347, Dec. 2016. DOI: 10.1109/JSEN.2016.2596712.

[18] E. A. Clancy, E. L. Morin, and R. Merletti, "Sampling, noise-reduction and amplitude estimation issues in surface electromyography," *J. of Electromyography and Kinesiology*, vol. 12, no. 1, pp. 1–16, Feb. 2002. DOI: 10.1016/S1050-6411(01)00033-5.

[19] L. Mesin, "Crosstalk in surface electromyogram: Literature review and some insights," *Physical and Engineering Sciences in Medicine*, vol. 43, no. 2, pp. 481–492, 2020. DOI: 10.1007/s13246-020-00868-1.

[20] G. L. Cerone, A. Botter, and M. Gazzoni, "A modular, smart, and wearable system for high density sEMG detection," *IEEE Transactions on Biomedical Engineering*, vol. 66, no. 12, pp. 3371–3380, Dec. 2019. DOI: 10.1109/TBME.2019.2904398.

[21] A. K. Sinha, D. D. Caviglia, and P. Gaur, "Design of an advanced signal conditioning unit for sensor with reduced off-the-shelf components," in *2012 International Conference on Devices, Circuits and Systems (ICDCS)*, 2012, pp. 316–319. DOI: 10.1109/ICDCSyst.2012.6188728.

[22] D. Esposito, V. Pizzella, G. Mercuri, P. M. Rossini, and F. Vernieri, "A smart approach to EMG envelope extraction and powerful denoising for human–machine interfaces," *Scientific Reports*, vol. 13, p. 19 600, 2023. DOI: 10.1038/s41598-023-33319-4.

[23] M. Simão, N. Mendes, O. Gibaru, and P. Neto, "A review on electromyography decoding and pattern recognition for human-machine interaction," *IEEE Access*, vol. 7, pp. 39 564–39 582, 2019. DOI: 10.1109/ACCESS.2019.2906584.